Z. Phys. B – Condensed Matter 74, 53–65 (1989)

Condensed
Zeitschrift für Physik B Matter
© Springer-Verlag 1989

# Barrier penetration effects for electrons in quantum wells: screening, mobility, and shallow impurity states

**A. Gold**
Groupe de Physique des Solides de l'Ecole Normale Supérieure, Université Paris 7, Paris, France

Received August 8, 1988

A two-dimensional electron gas in a quantum well confined by finite barriers is considered. We present analytical expressions for the finite confinement effects of a square-well potential and calculate the electron-electron interaction potential, the electron-impurity interaction potential, the interface-roughness scattering potential and the alloy-disorder scattering potential. The dielectric function of the interacting electron gas, the mobility (for charged-impurity scattering, for interface-roughness scattering, and for alloy-disorder scattering), and the binding energy of hydrogenic impurities (screened and unscreened) are discussed.

## I. Introduction

The calculations of electronic properties of silicon metal-oxide-semiconductor structures are usually made in the infinite barrier approximation due to the large barrier of 3.14 eV between the silicon conduction band and the silicon-dioxide conduction band [1]. In one-dimensional periodic structures such as quantum wells (QW's) and superlattices such as $Al_xGa_{1-x}As/GaAs$ the confining barrier height is between 1.0 eV for $x=1$ and 0 for $x=0$ [2]. In this case the finite confinement becomes very important and the penetration of the electron gas into the barrier can be studied in the III–V compound QW's and superlattices.

Charged impurities play a fundamental role in the understanding of the electronic properties of QW's. Mobility limits for charged impurity scattering in QW's have been discussed in the literature [3–6]. In order to calculate the mobility one needs to know the Fourier transform of the random potential and of the screening function [1, 7]. In the infinite barrier approximation analytical results have been given for silicon metal-oxide-semiconductor structures [7] and for quantum wells [4]. For finite barriers only numerical results are available [3, 5, 6]. In this paper we calculate the random potential for charged-impurity scattering and the electron-electron interaction potential for QW's with finite barriers and with finite width, and we derive analytical results. The results of the finite confinement on the mobility are discussed. The screening properties of the two-dimensional interacting electron gas which are fundamental to many other calculations (excitons, electron-phonon interaction, hot electrons) and which are determined by the electron-electron interaction potential, are calculated in this paper.

The finite confinement in QW's has already been used to explain the mobility of thin quantum wells where the interface-roughness scattering is dominant [8]. For infinite barriers the mobility $\mu$ for interface-roughness scattering was predicted to vary with the quantum well width $L$ as $\mu=\text{constant}*L^6$ [4]. Experiments on AlAs/GaAs/AlGa QW's exhibit a relatively low mobility [9], whereas the $Al_xGa_{1-x}As/GaAs/Al_xGa_{1-x}As$ QW's with $x\approx0.3$ showed a much higher mobility for comparable parameters such as electron density and QW width [8]. It was argued that the penetration of the wave function into the barrier reduces the interface-roughness scattering [8]. Analytical results for the mobility due to interface-roughness scattering are derived and discussed in this paper.

Alloy-disorder scattering for $Al_xGa_{1-x}As/GaAs/Al_xGa_{1-x}As$ QW's was first studied by Ando [10]. It is worthwhile mentioning that alloy-disorder scat-

tering is not present in the infinite-barrier approximation: The wave function does not penetrate into the $Al_xGa_{1-x}As$. However, interface-roughness scattering is strongest in this case. With decreasing confinement one expects alloy-disorder scattering to increase due to the larger penetration of the wave function into the barrier. In case of $InP/Ga_{1-x}In_xAs/InP$ QW's, where the electron gas and the alloy disorder are not separated in space, alloy-disorder scattering is present even in the infinite barrier approximation and becomes weaker for finite confinement [11]. In the present paper we present some analytical results for alloy-disorder scattering in QW's, and we discuss the effect of the finite confinement.

The calculations of the shallow hydrogenic impurity energy levels gave evidence of finite barrier effects in thin QW's [12–16]. The penetration of the electron wave function into the barrier reduces the binding energy for impurities in the center of QW's in comparison to QW's with infinite barriers [17]. For a review on experimental results of the binding energy of hydrogenic impurities in two-dimensional structures, see Ref. 18.

In a recent work the density of states in silicon metal-oxide-semiconductor structures in the presence of randomly distributed charged impurities has been studied [19]. The binding energy of hydrogenic impurities has been calculated within the separable potential approximation (SPA) and for an infinite barrier at the silicon/silicon-dioxide interface. In this approach the binding energy is given by a $q$-integral over the electron-impurity interaction potential (possibly screened). A very recent calculation within the SPA for the binding energy of shallow impurities in QW's with infinite barriers [20] was in good agreement with the calculation of Bastard [17]. In this paper we show that the calculation of the binding energy within the SPA for QW's with finite barriers, by using the analytical expression for the electron-impurity interaction potential, is also in reasonable agreement with the variational approach used in [12–16].

Our approach to calculate the binding energy for hydrogenic impurities uses exactly the same random potential that is used for the calculation of the scattering time [3–7] and the single particle relaxation time [21–23]. Our presentation of analytical formulas for the electron-impurity interaction potential provides a unified theoretical frame for the calculation of binding energies and transport properties in QW's with finite barriers.

The purpose of the present paper is to derive analytical formulas for a transparent understanding of finite barrier effects on the electronic properties (screening and mobility) of QW's. The calculations of the binding energies of hydrogenic impurities are extensive, because we want to show the good agreement with the variational calculations, and because we suggest that our approach can be used to get qualitative and quantitative results for the binding energy of hydrogenic impurities in geometries other than the square-well confinement considered in this paper.

The paper is organized as follows: In Sect. II we present the theoretical frame of our calculations (the model and the theory). Our results for the screening function, the mobility and the binding energy of hydrogenic impurities are given in Sect. III. We conclude in Sect. IV.

## II. Theoretical frame

In this section we present the model, the analytical results for the electron-electron interaction potential, the electron-impurity interaction potential, the interface-roughness scattering potential, and the alloy-disorder scattering potential.

### *A. The square well*

We consider a QW of width $L$ and effective barrier height $V$. Band bending effects are neglected, but the Pauli principle is taken into account; $V$ is given by the height of the barrier $V_0$ and the Fermi energy $\varepsilon_F$: $V = V_0 - \varepsilon_F$. Free motion of the electrons in the $xy$-plane is assumed, while the confinement is along the $z$-direction. The barriers are at $z = \pm L/2$ (see the inset of Fig. 1). We use parameters for $Al_xGa_{1-x}As/GaAs/Al_xGa_{1-x}As$ QW's with

$$V_0 = 1.04\ \mathrm{eV} * x. \tag{1}$$

For the electron masses in $z$-direction we take for the mass in the barrier $m_b$

$$m_b/m_0 = 0.067 + 0.071 * x \tag{2a}$$

and for the mass in the well $m_z$

$$m_z/m_0 = 0.067. \tag{2b}$$

$m_0$ is the vacuum mass of the electron. Due to the confinement in $z$-direction a subband structure $n = 1, 2, 3\ldots$ is defined. The wave function in $z$-direction decays exponentially in the barrier

$$\Phi_n(V, L, z) = \begin{cases} B_1\, e^{2\beta z/L} & \text{for } z < -L/2 \\ B_2\, e^{-2\beta z/L} & \text{for } z > L/2 \end{cases} \tag{3a}$$

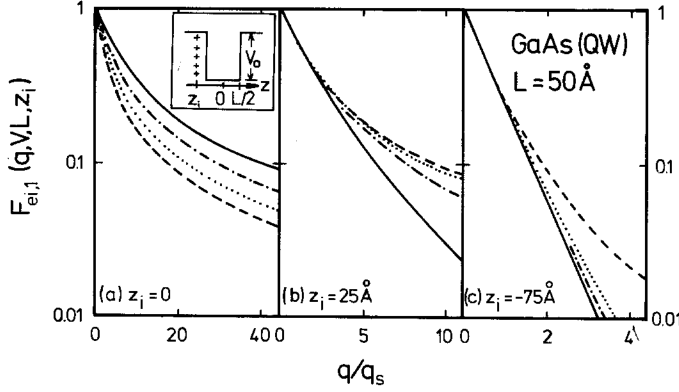


**Fig. 1a–c.** Form factor $F_{ei,1}(q, V, L, z_i)$ for the electron-impurity interaction potential (see (6)), for the lowest subband according to (7) versus wave number $q$ for impurities located (**a**) in the center of the QW, (**b**) on the edge of the QW, and (**c**) in the barrier. Solid, dashed-dotted, dotted and dashed lines represent $V$[eV] $= \infty$, 1, 0.3, and 0.1, respectively. The inset shows the position of impurities from the center of the QW and the height of the barrier $V_0$. The effective barrier height is $V = V_0 - \varepsilon_F$. $\varepsilon_F$ is the Fermi energy. In cases where we do not specify $V_0$ we use $V = V_0$. $q_s$ is the Thomas-Fermi screening wave number

and is characterized by

$$\Phi_n(V, L, z) = \begin{cases} A_1 * \cos(2\alpha z/L) & n = 1, 3, 5 \ldots \\ A_2 * \sin(2\alpha z/L) & n = 2, 4, 6 \ldots \end{cases} \quad \text{for } -L/2 \leqq z \leqq L/2. \tag{3b}$$

The normalization coefficients $A_1$, $A_2$, $B_1$, and $B_2$ are given later.

The energy levels $E_n$ (measured from the bottom of the well) are expressed as

$$E_n = 2\hbar^2 \alpha^2 / L^2 m_z \tag{4}$$

and $\alpha$ for $\pi(n-1)/2 < \alpha \leqq \pi n/2$ is given by

$$(m_z/m_b)^{1/2} (C - \alpha^2)^{1/2} = \begin{cases} \alpha * \tan(\alpha) & \text{for } n = 1, 3, 5 \ldots \\ -\alpha/\tan(\alpha) & \text{for } n = 2, 4, 6 \ldots \end{cases} \tag{5a}$$

and

$$C = \frac{1}{4} \frac{m_z}{m^*} \frac{L^2}{a^{*2}} \frac{V}{R}. \tag{5b}$$

$m^* = 0.067\, m_0$ is the mass in the $xy$-plane, $a^* = \varepsilon_L \hbar^2 / m^* e^2 = 103$ Å is the effective Bohr radius and $R = m^* e^4 / 2\varepsilon_L^2 \hbar^2 = 5.6$ meV is the effective Rydberg. $\varepsilon_L = 13.1$ is the dielectric constant of the host lattice. The penetration into the barrier is characterized by $\beta$ and given by

$$\frac{m_z}{m_b} \beta = \begin{cases} \alpha \tan(\alpha) & \text{for } n = 1, 3, 5 \ldots \\ -\alpha/\tan(\alpha) & \text{for } n = 2, 4, 6 \ldots \end{cases}. \tag{5c}$$

For QW's with infinite barriers one finds $\alpha = \pi n/2$ and $1/\beta = 0$.

*B. The electron-impurity interaction potential*

We assume a two-dimensional sheet of charged impurities which are distributed randomly in the $xy$-plane at a distance $z_i$ from the center of the QW which is at $z = 0$. $N_i$ is the impurity density. The Fourier transform of the random potential for the subband $n \langle |U_n(q, V, L, z_i)|^2 \rangle$, which is induced by the impurity sheet, is written as [1]

$$\langle |U_n(q, V, L, z_i)|^2 \rangle = N_i\, V_{ei,n}(q, V, L, z_i)^2 \tag{6a}$$

with

$$V_{ei,n}(q, V, L, z_i) = \frac{2\pi e^2}{\varepsilon_L q} F_{ei,n}(q, V, L, z_i) \tag{6b}$$

and

$$F_{ei,n}(q, V, L, z_i) = \int_{-\infty}^{+\infty} dz\, |\Phi_n(V, L, z)|^2\, e^{-q|z - z_i|}. \tag{6c}$$

We have calculated $F_{ei,n}(q, V, L, z_i)$ for the square-well confinement in terms of $\alpha$ and $\beta$ and the result for $n = 1, 3, 5 \ldots$ is written as

$$\begin{aligned} &F_{ei,n}(q, V, L, -L/2 < z_i < L/2) \\ &= 4A_o \Bigg\{ \cos^2(\alpha)\, \mathrm{ch}(q z_i)\, e^{-qL/2} \frac{1}{qL + 4\beta} \\ &+ \frac{qL}{(qL)^2 + 16\alpha^2} \Bigg[ \cos^2(2\alpha z_i/L) \\ &+ \frac{8\alpha^2}{(qL)^2} (1 - \mathrm{ch}(q z_i)\, e^{-qL/2}) \\ &- e^{-qL/2} \cos(\alpha)\, \mathrm{ch}(q z_i) \left( \cos(\alpha) - \frac{4\alpha}{qL} \sin(\alpha) \right) \Bigg] \Bigg\} \end{aligned} \tag{7a}$$

and

$$\begin{aligned} &F_{ei,n}(q, V, L, z_i \leqq -L/2) \\ &= 4A_o \Bigg\{ \frac{1}{(qL)^2 + 16\alpha^2} e^{q z_i} * \Bigg[ \cos(\alpha)(qL \cos(\alpha)\, \mathrm{sh}(qL/2) \\ &+ 4\alpha \sin(\alpha)\, \mathrm{ch}(qL/2)) + \frac{8\alpha^2}{qL} \mathrm{sh}(qL/2) \Bigg] \\ &+ \cos^2(\alpha) \Bigg[ \frac{1}{2(qL + 4\beta)} e^{q(z_i - L/2)} + \frac{qL}{(qL)^2 - 16\beta^2} \\ &* e^{2\beta(1 + 2z_i/L)} - \frac{1}{2(qL - 4\beta)} e^{q(z_i + L/2)} \Bigg] \Bigg\} \end{aligned} \tag{7b}$$

and $F_{ei}(q, V, L, z_i \geqq L/2)$ is given by replacing $z_i$ by $-z_i$ in (7b). $A_o$ is written as

$$A_o = \frac{1}{1+\sin(2\alpha)/(2\alpha)+\cos^2(\alpha)/\beta}. \tag{7c}$$

The normalization coefficients in (3) for $n=1, 3, 5\ldots$ are expressed as: $A_1=(2A_o/L)^{1/2}$ and $B_1=B_2 = A_1 \cos(\alpha)\exp(\beta)$. For $n=2, 4, 6\ldots$ we get

$$\begin{aligned} &F_{ei}(q, V, L, -L/2<z_i<L/2)\\ &=4A_e\left\{\sin^2(\alpha)\,\mathrm{ch}(qz_i)\,\mathrm{e}^{-qL/2}\frac{1}{qL+4\beta}\right.\\ &\quad+\frac{qL}{(qL)^2+16\alpha^2}\left[\sin^2(2\alpha z_i/L)\right.\\ &\quad+\frac{8\alpha^2}{(qL)^2}(1-\mathrm{ch}(qz_i)\,\mathrm{e}^{-qL/2})\\ &\quad\left.\left.-\mathrm{e}^{-qL/2}\sin(\alpha)\,\mathrm{ch}(qz_i)\left(\sin(\alpha)+\frac{4\alpha}{qL}\cos(\alpha)\right)\right]\right\} \end{aligned} \tag{8a}$$

and

$$\begin{aligned} &F_{ei,n}(q, V, L, z_i \leqq -L/2)\\ &=4A_e\left\{\frac{1}{(qL)^2+16\alpha^2}\,\mathrm{e}^{qz_i}*\left[\sin(\alpha)(qL\sin(\alpha)\,\mathrm{sh}(qL/2)\right.\right.\\ &\quad-4\alpha\cos(\alpha)\,\mathrm{ch}(qL/2))\\ &\quad\left.+\frac{8\alpha^2}{qL}\,\mathrm{sh}(qL/2)\right]\\ &\quad+\sin^2(\alpha)\left[\frac{1}{2(qL+4\beta)}\,\mathrm{e}^{q(z_i-L/2)}+\frac{qL}{(qL)^2-16\beta^2}\right.\\ &\quad\left.\left.*\,\mathrm{e}^{2\beta(1+2z_i/L)}-\frac{1}{2(qL-4\beta)}\,\mathrm{e}^{q(z_i+L/2)}\right]\right\} \end{aligned} \tag{8b}$$

and $F_{ei}(q, V, L, z_i \geqq L/2)$ is given by replacing $z_i$ by $-z_i$ in (8b). $A_e$ is written as

$$A_e = \frac{1}{1-\sin(2\alpha)/(2\alpha)+\sin^2(\alpha)/\beta}. \tag{8c}$$

The normalization coefficients in (3) for $n=2, 4, 6\ldots$ are expressed: $A_2=(2A_e/L)^{1/2}$ and $B_1=-B_2= -A_2\sin(\alpha)\exp(\beta)$. The form factor for $n=1$ and for infinite barriers was given in [4].

In Fig. 1 we have calculated the form factor $F_{ei,n}(q, V, L, z_i)$ for the lowest subband $n=1$ versus $q$ for various values of $V$ and three values of $z_i$: a) $z_i=0$ (impurities in the center of the QW), b) $z_i=L/2$ (impurities on the edge of the QW), c) $z_i=-3L/2$ (impurities in the barrier of the QW). For impurities in the center of the QW the electron-impurity interaction potential is reduced by the finite barriers due to the penetration of the electron wave function into the barriers and the corresponding reduction of the electron probability at $z=0$. For impurities in the barrier of the QW the electron impurity interaction potential is enhanced due to the penetration of the electron wave function into the barrier.

### *C. The electron-electron interaction potential*

The electron-electron interaction potential $V_{c,n}(q, V, L)$ is expressed as [1]

$$V_{c,n}(q, V, L) = \frac{2\pi e^2}{\varepsilon_L q} F_{c,n}(q, V, L) \tag{9a}$$

with

$$\begin{aligned} &F_{c,n}(q, V, L)\\ &=\int_{-\infty}^{+\infty}\mathrm{d}z|\Phi_n(V, L, z)|^2\int_{-\infty}^{+\infty}\mathrm{d}z'|\Phi_n(V, L, z')|^2\,\mathrm{e}^{-q|z-z'|}. \end{aligned} \tag{9b}$$

We have calculated the form factor $F_{c,n}(q, V, L)$ for the electron-electron interaction potential for the square-well confinement. For $n=1, 3, 5\ldots$ we find

$$\begin{aligned} &F_{c,n}(q, V, L)\\ &=2A_o^2\left\{\cos^4(\alpha)\left[\mathrm{e}^{-qL}\frac{4}{(qL+4\beta)^2}+\frac{1}{\beta(qL+4\beta)}\right]\right.\\ &\quad+\frac{qL}{\alpha((qL)^2+16\alpha^2)}\left[\frac{3}{2}\alpha+16\frac{\alpha^3}{(qL)^2}+\left(\frac{3}{2}+16\frac{\alpha^2}{(qL)^2}\right)\right.\\ &\quad\left.*\sin(\alpha)\cos(\alpha)+\sin(\alpha)\cos^3(\alpha)\right]\\ &\quad+\frac{8\alpha}{(qL)^2+16\alpha^2}\left[\cos(\alpha)\left(\frac{qL}{\alpha}\cos(\alpha)\,\mathrm{sh}(qL/2)\right.\right.\\ &\quad\left.\left.+4\sin(\alpha)\,\mathrm{ch}(qL/2)\right)+\frac{8\alpha}{qL}\mathrm{sh}(qL/2)\right]\\ &\quad*\,\mathrm{e}^{-qL/2}\left[\frac{2\cos^2(\alpha)}{qL+4\beta}-\frac{1}{(qL)^2+16\alpha^2}\right.\\ &\quad\left.\left.*\left(8\frac{\alpha^2}{qL}+qL\cos^2(\alpha)-4\alpha\sin(\alpha)\cos(\alpha)\right)\right]\right\} \end{aligned} \tag{10}$$

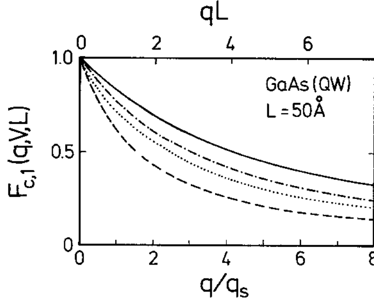


**Fig. 2.** Form factor $F_{c,1}(q, V, L)$ for the electron-electron interaction potential (see (9)), for the lowest subband according to (10) versus wave number $q$. Solid, dashed-dotted, dotted, and dashed lines represent $V[\mathrm{eV}] = \infty$, 1, 0.3, 0.1, respectively

and for $n = 2, 4, 6 \ldots$ we get

$$\begin{aligned} &F_{c,n}(q, V, L) \\ &= 2A_e^2 \Big\{ \sin^4(\alpha) \Big[ e^{-qL} \frac{4}{(qL+4\beta)^2} + \frac{1}{\beta(qL+4\beta)} \Big] \\ &+ \frac{qL}{\alpha((qL)^2+16\alpha^2)} \Big[ \frac{3}{2}\alpha + 16\frac{\alpha^3}{(qL)^2} - \Big(\frac{3}{2} + 16\frac{\alpha^2}{(qL)^2}\Big) \\ &* \sin(\alpha)\cos(\alpha) - \sin^3(\alpha)\cos(\alpha) \Big] \\ &+ \frac{8\alpha}{(qL)^2+16\alpha^2} \Big[ \sin(\alpha) \Big( \frac{qL}{\alpha} \sin(\alpha)\,\mathrm{sh}(qL/2) \\ &- 4\cos(\alpha)\,\mathrm{ch}(qL/2) \Big) + \frac{8\alpha}{qL}\mathrm{sh}(qL/2) \Big] \\ &* e^{-qL/2} \Big[ \frac{2\sin^2(\alpha)}{qL+4\beta} - \frac{1}{(qL)^2+16\alpha^2} \\ &* \Big( 8\frac{\alpha^2}{qL} + qL\sin^2(\alpha) - 4\alpha\sin(\alpha)\cos(\alpha) \Big) \Big] \Big\}. \qquad (11) \end{aligned}$$

The form factor for the lowest subband $n = 1$ and for infinite barriers was given in [4].

In Fig. 2 we show $F_{c,1}(q, V, L)$ versus $q$ for various values for the confining potential. For $L = 0$ and $V = \infty$ we get: $F_{c,1}(q, V = \infty, L = 0) = 1$. For finite $V$ and $q$ we find $F_{c,1}(q, V, L) < 1$. This indicates that the screening properties of the interacting electron gas are reduced by the finite confinement and the finite QW width.

*D. The interface-roughness scattering potential*

The decrease in the electron mobility in silicon metal-oxide-semiconductor structures at high electron density is due to the interface-roughness of the silicon/silicon-dioxide interface [1]. The local deviations from a plane $\delta z(\mathbf{r})$ are described by the autocorrelation function $\langle \delta(\mathbf{r})\,\delta(\mathbf{r}') \rangle = \Delta^2 \exp(-|\mathbf{r}-\mathbf{r}'|^2/\Lambda^2)$. $\Delta$ is the height of the roughness and $\Lambda$ is the length of the roughness fluctuations. This form of interface-roughness scattering was introduced by Prange and Nee [24] in the field of magnetic-field induced surface states in metals.

For QW's with infinite barriers the random potential for interface-roughness scattering of electrons at $z = \pm L/2$ in the lowest subband $\langle |U_{IR,1}(q, V = \infty, L)|^2 \rangle$ was expressed as [4]

$$\langle |U_{IR,1}(q, V = \infty, L)|^2 \rangle = \pi\Delta^2\Lambda^2 F_0(L)^2 e^{-q^2\Lambda^2/4}, \qquad (12a)$$

$$F_0(L) = \frac{\pi^2\hbar^2}{m_z L^3}. \qquad (12b)$$

According to this expression the mobility in thin QW's was predicted to vary as $\mu = \text{constant} * L^6$. Interface-roughness scattering for finite barriers was considered by Price and Stern [25]. The random potential for interface-roughness scattering at $z = -L/2$ is written as

$$\begin{aligned} &\langle |U_{IR,n}(q, V, L)|^2 \rangle \\ &= \pi\Delta^2\Lambda^2 F_n(V, L)^2 F_0(L)^2 e^{-q^2\Lambda^2/4} \end{aligned} \qquad (13a)$$

and [25]

$$\begin{aligned} &F_n(V, L)\, F_0(L) \\ &= \frac{\hbar^2}{2m_z}\Big(1 - \frac{m_b}{m_z}\Big)\Big(\frac{d\Phi_n}{dz}\Big)^2_{z=-L/2+\varepsilon} \\ &+ V|\Phi_n(z = -L/2)|^2. \end{aligned} \qquad (13b)$$

For the square-well confining potential we find for $n = 1, 3, 5 \ldots$

$$\begin{aligned} F_n(V, L) = \frac{4}{\pi^2}\Big\{ &\Big(1 - \frac{m_b}{m_z}\Big)\alpha^2\sin^2(\alpha) \\ &+ C * \cos^2(\alpha) \Big\} A_o \end{aligned} \qquad (14)$$

and for $n = 2, 4, 6 \ldots$

$$\begin{aligned} F_n(V, L) = \frac{4}{\pi^2}\Big\{ &\Big(1 - \frac{m_b}{m_z}\Big)\alpha^2\cos^2(\alpha) \\ &+ C * \sin^2(\alpha) \Big\} A_e \end{aligned} \qquad (15)$$

and $C$ was given in (5b). For $V = \infty$ we get $F_n(V = \infty, L) = n^2$. The asymptotic results for $F_n(V, L)$ are given by

$$F_n(V, L) = n^2 \Big\{ 1 - 3\Big[\frac{m_b}{m_z}\frac{1}{C}\Big]^{1/2} + O(1/C) \Big\}$$

$$\text{for } C^2 \gg m_b/m_z \qquad (16)$$

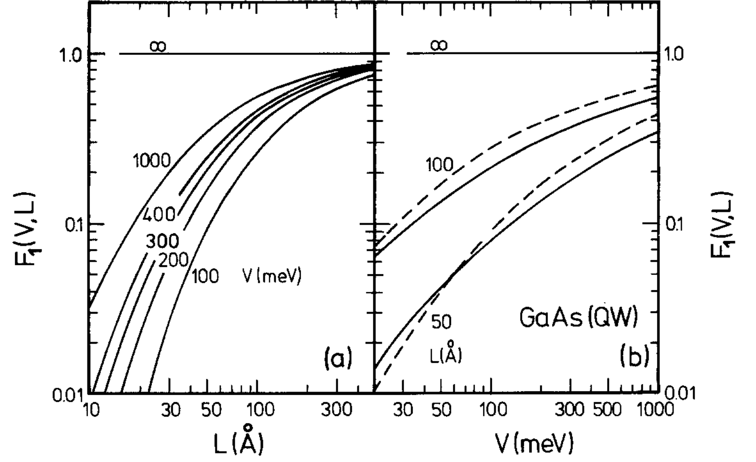


**Fig. 3a and b.** Form factor $F_1(V, L)$ for interface-roughness scattering (see (13)), for the lowest subband according to (14) (**a**) versus quantum well width $L$ for various values for the confining potential $V$ and (**b**) versus confining potential $V$ for various values of $L$. The dashed and solid lines represent $m_b = m_z$ and $m_b = 2.06\, m_z$, respectively

and

$$F_1(V, L) = \frac{1}{\pi^2} \frac{m_b}{m_z} C^2 \quad \text{for } C \to 0 \tag{17a}$$

and

$$F_{n \geqq 2}(V, L) = 0 \quad \text{for } C^{1/2} \leqq \pi(n-1)/2. \tag{17b}$$

Equation (17b) represents the minimal confinement condition for the existence of higher subbands with $n \geqq 2$.

In Fig. 3 we have shown $F_1(V, L)$ versus $L$ for various values of $V$ (Fig. 3a) and versus $V$ for various values of $L$ (Fig. 3b). The dashed lines in Fig. 3b represent $m_b = m_z$ ($x=0$) and the solid lines represent $m_b = 2.06\, m_z$ ($x=1$) (see (2)). The penetration of the wave function into the barrier drastically reduces, via $F_1(V, L)$, the interface-roughness scattering potential for thin QW's (see Fig. 3a). The change in the mass at the interface has a considerable effect on the interface-roughness scattering potential (see Fig. 3b). Figure 3b can also be used to estimate the effect of increasing electron density on the form factor $F_1(V, L)$ via $V = V_0 - \varepsilon_F$. The finite barrier effect was applied in [8] to explain the high mobility in $Al_xGa_{1-x}As/GaAs/Al_xGa_{1-x}As$ QW's with $x \approx 0.3$ in comparison to AlAs/GaAs/AlAs QW's [9].

### *E. The alloy-disorder scattering potential*

Alloy-disorder scattering in $Al_xGa_{1-x}As/GaAs$ heterostructures was found to be unimportant in comparison to charged-impurity scattering [10]. Ando [10] argued that one cannot distinguish between interface-roughness scattering and alloy-disorder scattering if the fluctuation of the interface position is comparable to the lattice constant. However, the experiments on QW's [8, 9] indicate that $\Lambda \approx 60$ Å. In the following we will derive the random potential for alloy-disorder scattering for large and small confining potentials. The QW width dependence of the scattering potential indicates that the scattering from the interface roughness is different to the scattering from the alloy disorder. Following Ando [10] we write the random potential for alloy-disorder scattering in the $n$-th subband as

$$\langle |U_{\mathrm{AD},n}(q, V, L)|^2 \rangle = \frac{1}{4} \frac{a^3}{a^*} (\delta V)^2 F_{\mathrm{AD},n}(V, L) \tag{18a}$$

and for QW's with the alloy disorder in the barrier $F_{\mathrm{AD},n}(V, L)$ is defined as

$$F_{\mathrm{AD},n}(V, L) = x(1-x)\, a^* \left\{ \int_{-\infty}^{-L/2} \mathrm{d}z\, |\Phi_n(V, L, z)|^4 + \int_{L/2}^{\infty} \mathrm{d}z\, |\Phi_n(V, L, z)|^4 \right\}. \tag{18b}$$

Explicitly we find

$$F_{\mathrm{AD},n}(V, L) = \frac{a^*}{L} \frac{x(1-x)}{\beta} \begin{cases} A_o^2 * \cos^4(\alpha) & \text{for } n = 1, 3, 5 \ldots \\ A_e^2 * \sin^4(\alpha) & \text{for } n = 2, 4, 6 \ldots \end{cases} \tag{19}$$

$\delta V$ is the spatial average of the fluctuating alloy potential over the alloy unit cell, $a^3$ is the alloy unit cell. We use: $\delta V = 1$ eV and $a = 5.9$ Å [10]. The asymptotic results for $F_{\mathrm{AD},1}(V, L)$ are given by

$$F_{\mathrm{AD},1}(V, L) = \frac{\pi^4}{16} \frac{a^*}{L} x(1-x) \left(\frac{m_b}{m_z}\right)^{3/2} * \frac{1}{C^{5/2}} \left\{ 1 - 2\left[\frac{m_b}{m_z} \frac{1}{C}\right]^{1/2} + O(1/C) \right\} \tag{20}$$

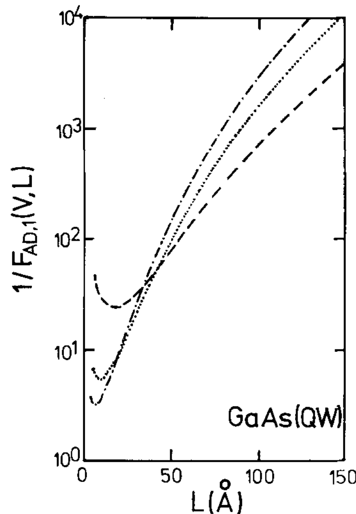


**Fig. 4.** Form factor $F_{AD,1}(V, L)$ for alloy-disorder scattering (see (18)), versus QW width $L$ according to (19) for various values of the confinement. The dashed-dotted, dotted, and dashed lines represent $V$[eV] = 0.5, 0.3, and 0.1, respectively

for $C^2 \gg (m_b/m_z)$ and

$$F_{AD,1}(V,L) = \frac{1}{4}\frac{a^*}{L}x(1-x)\frac{m_b}{m_z} \cdot C\left\{1 - C\left[\frac{1}{2} + \frac{m_b}{m_z}\right] + O(C^2)\right\} \quad (21)$$

for $C \to 0$.

In Fig. 4 we have shown $1/F_{AD,1}(V, L)$ versus the QW width for various confining potentials. The strong increase in $F_{AD,1}$ with decreasing $L$ (for $L > 20$ Å) indicates the increasing alloy-disorder scattering due to the larger penetration of the wave function into the barrier with decreasing $L$. For small QW width ($L < 10$ Å) a decrease in $F_{AD,1}$ with decreasing QW width is found, which can also be seen from (21).

For reasons of completeness we are now discussing the case where the alloy-disorder scattering occurs in the QW. In this case $F_{AD,1}(V, L)$ is defined by

$$F_{AD,n}(V,L) = x(1-x)\,a^*\left\{\int_{-L/2}^{L/2} \mathrm{d}z\,|\Phi_n(V,L,z)|^4\right\}. \quad (22)$$

We get the analytical result

$$F_{AD,n}(V,L) = \frac{3}{2}\frac{a^*}{L}x(1-x) \cdot \begin{cases} A_o^2\left[1 + \dfrac{2\sin(2\alpha)}{3\alpha} + \dfrac{\sin(4\alpha)}{12\alpha}\right] & \text{for } n = 1, 3 \ldots \\ A_e^2\left[1 - \dfrac{2\sin(2\alpha)}{3\alpha} + \dfrac{\sin(4\alpha)}{12\alpha}\right] & \text{for } n = 2, 4 \ldots \end{cases} \quad (23)$$

The asymptotic results for the lowest subband are given by

$$F_{AD,1} = \frac{3}{2}\frac{a^*}{L}x(1-x)\left\{1 - 3\left[\frac{m_b}{m_z}\frac{1}{C}\right]^{1/2} + O(1/C)\right\}$$

for $C^2 \gg m_b/m_z$ (24)

and

$$F_{AD,1} = \frac{3}{2}\frac{a^*}{L}x(1-x)\frac{m_b^2}{m_z^2}C^2$$

for $C \to 0$. (25)

It is obvious from (24) that alloy-disorder scattering exists even in the limit of $V \to \infty$ ($C \to \infty$), for alloy scattering in the barrier, however, the opposite is true. For AlAs/GaAs/AlAs QW's the alloy-disorder scattering does not exist because $x = 1$.

## III. Results and discussion

In this section we apply our results for the various form factors, given in Sect. II, to calculate the effects of the confinement on the screening properties of the interacting electron gas, the mobility due to charged-impurity scattering, interface-roughness scattering, alloy-disorder scattering, and the binding energy of screened and unscreened hydrogenic impurities.

### *A. Screening properties of the electron gas*

In the random phase approximation [1] with local field (exchange-correlation) correlation the dielectric function in the one-subband approximation $\varepsilon(q, V, L)$ is written as

$$\varepsilon(q, V, L) = 1 + V_{c,1}(q, V, L)[1 - G(q)]\,X^0(q). \quad (26)$$

$X^0(q)$ is the Lindhard function for two dimensions [1, 26]. For the local field correction $G(q)$ we use the Hubbard approximation [27]. For an ideally two-dimensional electron gas, which is characterized by $L = 0$ and $V = \infty$, the dielectric function is given by

$$\varepsilon_{\text{ideal}}(q) = 1 + \frac{q_s}{q}[1 - G(q)]\frac{X^0(q)}{\sigma_F}. \quad (27)$$

$q_s$ is the Thomas-Fermi screening wave number: $q_s a^* = 2$ for valley degeneracy $g_v = 1$. $\sigma_F$ is the density of states of the free electron gas: $X^0(q)/\sigma_F = 1$ for $q \leqq 2k_F$ and $k_F$ is the Fermi wave number.

The transport properties of the two-dimensional-electron gas for a short-range random potential are determined by the screening properties at $q \cong 2k_F$ [28]. In Fig. 5 we have shown $\varepsilon(q = 2k_F, V, L)/\varepsilon_{\text{ideal}}(q = 2k_F)$ versus $L$ for two different electron densities $N = k_F^2/2\pi$ and for various confinements. The screening properties of the electron gas are reduced for QW's with finite width as well as for QW's with finite confinement. With increasing electron density

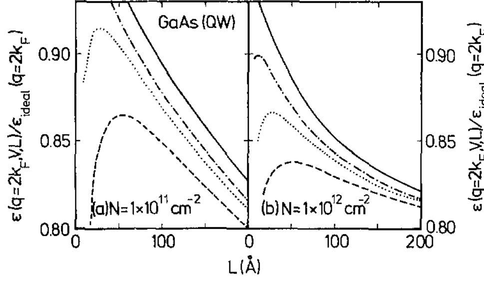


**Fig. 5a and b.** Ratio of screening functions $\varepsilon(q=2k_F, V, L)/\varepsilon_{\mathrm{ideal}}(q=2k_F)$ according to (26), (27) versus QW width $L$ for electron density (**a**) $N=1*10^{11}$ cm$^{-2}$ and (**b**) $N=1*10^{12}$ cm$^{-2}$. Solid, dashed-dotted, dotted and dashed lines represent $V$[eV] $=\infty$, 1, 0.3, 0.1, respectively

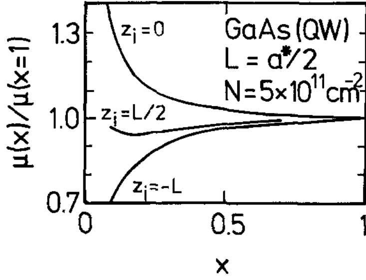


**Fig. 6.** Mobility ratio $\mu(x)/\mu(x=1)$ versus aluminium content $x$ (confining potential, (see Eq. (1))) for charged impurity scattering according to (6, 7, 28) for impurities located in the center ($z_i=0$), on the edge ($z_i=+L/2$) of the QW, and in the barrier ($z_i=-L$)

the reduction in the screening properties becomes larger. However, the effect is smaller than 20% for QW's with $L<100$ Å. If we compare the dielectric function for finite confinement with the screening function for infinite confinement, we find that the two differ by only about 10% for $L<200$ Å. However, we mention that the finite QW width and the finite confinement drastically reduce the screening properties at large wave numbers if compared with the screening properties of an ideally two-dimensional electron gas (see Fig. 2).

*B. Mobility for charged-impurity scattering, interface-roughness scattering, and alloy-disorder scattering*

The scattering time $\tau$ determines the mobility $\mu$: $\mu=e\tau/m^*$. In terms of the random potential $\langle|U(q)|^2\rangle$ the scattering time for electrons in the lowest subband is given by [7]

$$\frac{1}{\tau}=\frac{1}{2\pi\varepsilon_F}\int_0^{2k_F} dq\,\frac{q^2}{(4k_F^2-q^2)^{1/2}}\,\frac{\langle|U(q)|^2\rangle}{\varepsilon(q)^2}. \tag{28}$$

For charged impurity scattering the random potential is given in (6), (7a). The mobility for $Al_xGa_{1-x}As/GaAs/Al_xGa_{1-x}As$ QW's versus $x$ (versus the confining potential (see (1))) is shown in Fig. 6.

**Table 1.** Absolute values of the mobility for impurity scattering for $N=5*10^{11}$ cm$^{-2}$, $N_i=1*10^{11}$ cm$^{-2}$ and $L=a^*/2$ (see Fig. 6)

| $V$(eV) | $\mu(z_i=0)\left(\frac{\mathrm{cm}^2}{Vs}\right)$ | $\mu(z_i=\pm L/2)\left(\frac{\mathrm{cm}^2}{Vs}\right)$ | $\mu(z_i=\pm L)\left(\frac{\mathrm{cm}^2}{Vs}\right)$ |
|---|---|---|---|
| 1.04 | $1.02*10^4$ | $2.04*10^4$ | $6.46*10^4$ |
| $\infty$ | $0.93*10^4$ | $2.27*10^4$ | $7.04*10^4$ |

For impurities located in the center of the QW ($z_i=0$) the mobility increases with decreasing $x$, whereas the opposite behavior is found for impurities located in the barrier ($z_i=-L$). For impurities located on the edge of the QW ($z_i=L/2$) a very weak $x$-dependence of the mobility is found. For silicon metal-oxide-semiconductors it was shown that $\mu\approx 1/F_{ei}(q=2k_F)^2$ [28]. The same behavior is found in QW's, compare Fig. 6 with Fig. 1. The absolute values for the mobility for $V=1.04$ eV ($x=1$) and for $V=\infty$ are given in Table 1. The difference in the mobility calculated in the infinite barrier approximation in comparison to $V=1.04$ eV is 10% for the parameters used in Table 1. For larger QW's this error is smaller due to less penetration into the barrier. Small finite confinement effects on the mobility for charged-impurity scattering have also been found for $Al_xGa_{1-x}As/GaAs$ heterostructures [10].

Finite barrier effects are also expected for the single particle relaxation time [21–23]. However, the finite barrier effects are expected to be somewhat larger than for the scattering time, because in the single particle relaxation time larger wave numbers (up to $2k_F$) have a larger weight than in the scattering time (see also Fig. 1).

The random potential for interface-roughness scattering is given in (13), (14). According to [28] we get the analytical results for scattering at one interface

$$\mu=2.64\,\frac{\mathrm{cm}^2}{Vs}\left(\frac{10^{11}\,\mathrm{cm}^{-2}}{N}\right)\left(\frac{L^6 q_s^2}{\Delta^2\Lambda^2}\right)\left(\frac{1}{F_1(V,L)}\right)^2 *\left\{[1-G(2k_F)]\,F_{c,1}(q=2k_F,V,L)+\frac{2k_F}{q_s}\right\}^2 \tag{29}$$

for $k_F\Lambda\ll 1$ and

$$\mu=2.34\,\frac{\mathrm{cm}^2}{Vs}\left(\frac{10^{11}\,\mathrm{cm}^{-2}}{N}\right)\left(\frac{L^6 q_s^2\Lambda^3 k_F^5}{\Delta^2}\right)\left(\frac{1}{F_1(V,L)}\right)^2 *\left\{[1-G(2/\Lambda)]\,F_{c,1}(q=2/\Lambda,V,L)+\frac{2}{q_s\Lambda}\right\}^2 \tag{29b}$$

for $k_F\Lambda\gg 1$. For $V=\infty$ the mobility depends on $L$ via the $L^6$ and $F_{c,1}(q, V=\infty, L)$. In Fig. 7 we have

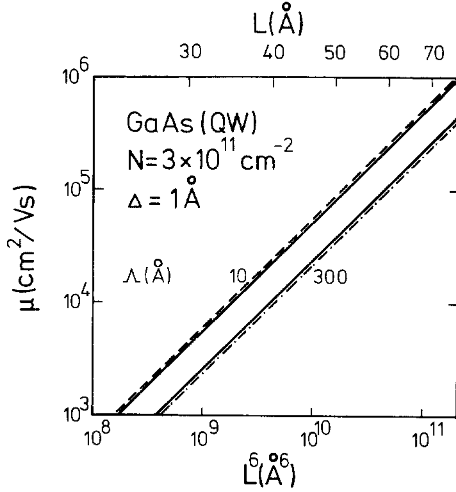


**Fig. 7.** Mobility $\mu$ versus $L^6$ ($L$ is the QW width) with the same interface-roughness parameters for both interfaces according to (12, 28) and infinite confinement. The dashed and dashed-dotted line represent Eqs. (29a), (29b), respectively

shown $\mu$ versus $L^6$ for infinite confinement. We find: $\mu = \text{constant} * L^6$. This demonstrates that for $\mu(L)$ there is no significant $L$ dependence due to $F_{c,1}(q, V=\infty, L)$ for $20\,\text{Å} < L < 80\,\text{Å}$. The dashed and dashed-dotted lines in Fig. 7 represent Eqs. (29a, b), respectively, and demonstrate the very good agreement of the analytical results with the numerical results.

For finite $V$ and for $L$ ($L_1 < L < L_2$) we can use the expression $F_1(V, L) \approx \text{constant} * L^\delta$, see Fig. 3, to express the mobility as $\mu = \text{constant} * L^{(6-2\delta)}$. Together with the analytical results, given in (16), (17a), we summarize: For interface-roughness scattering the QW width dependence of the mobility is expressed as

$$\mu \propto \begin{cases} L^6 V^0 & \text{for } C \to \infty \\ L^{-2} V^{-2} & \text{for } C \to 0 \end{cases} \tag{30}$$

The increase in the mobility with decreasing QW width is due to the delocalization of the wave function in $z$-direction if the confinement goes to zero. This is visible in Fig. 3: For small confinement we find $F_1(V, L) \propto L^\delta$ with $\delta > 3$.

For reasons of physical interpretation one expects the interface-roughness parameter $\Delta$ to be a multiple of a monolayer which is 2.83 Å. Because of the scaling law $\mu = \text{const} * 1/\Delta^2$ we have used $\Delta = 1$ Å in Fig. 7. We have also assumed in Fig. 7 that both interfaces contribute to the interface-roughness scattering with the same interface-roughness parameters. In this case the random potential, given in (12), (13), must be multiplied by two and the analytical results for the mobility, given in (29), must be divided by two.

The random potential for alloy-disorder scattering is given in (18), (19). Following [28] we get the analytical result

$$\mu = 1.69 * 10^8 \frac{\text{cm}^2}{Vs} \left(\frac{10^{11}\,\text{cm}^{-2}}{N}\right) \left(\frac{1}{\delta V[\text{eV}]}\right)^2 \cdot \left(\frac{1}{a^*[\text{Å}]}\right)^4 \left(\frac{a^*}{a}\right)^3 * \frac{1}{F_{\text{AD},1}(V, L)} \cdot \left\{[1 - G(2k_F)]\, F_{c,1}(q = 2k_F, V, L) + \frac{2k_F}{q_s}\right\}^2 \tag{31}$$

and the $V$ and $L$ dependence is hidden in $F_{\text{AD},1}(V, L)$ and in $F_{c,1}(q, V, L)$. We summarize the QW width dependence of the mobility for alloy-disorder scattering in the barrier (see (20), (21)):

$$\mu \propto \begin{cases} L^6 V^{5/2} & \text{for } C \to \infty \\ L^{-1} V^{-1} & \text{for } C \to 0 \end{cases}. \tag{32}$$

For strong confinement we find the same dependence on QW width as for interface-roughness scattering with infinite barriers (see (30)). The $V^{5/2}$ dependence was also found for heterostructures [10]. The strong $L$ dependence for alloy-disorder scattering has also been found in [29], however, analytical results have not been given there. The increase in $\mu$ with decreasing $L$ for weak confinement is due to the increased barrier penetration and thus to the decreased sensitivity to spatial fluctuations which occur on the fixed scale of the unit cell.

This argument is also important for the understanding of the mobility in the case where the alloy-disorder scattering occurs in the QW. For alloy scattering in the QW we get with (24, 25)

$$\mu \propto \begin{cases} L^1 V^0 & \text{for } C \to \infty \\ L^{-3} V^{-3} & \text{for } C \to 0 \end{cases}. \tag{33}$$

The divergency of the alloy-disorder limited mobility for $L \to 0$ has been noticed in [11]; however, the analytical form has not been derived and the screening of the alloy-disorder scattering has not been taken into account in [11]. The $\mu \propto L$ dependence reflects the decreasing confinement of the wave function if the QW width increases [11].

In Fig. 8 we show the mobility for interface-roughness scattering and for alloy-disorder scattering versus QW width. It can clearly be seen that interface-roughness scattering gives a lower mobility than alloy-disorder scattering and thus is the dominant scattering mechanism for thin QW's.

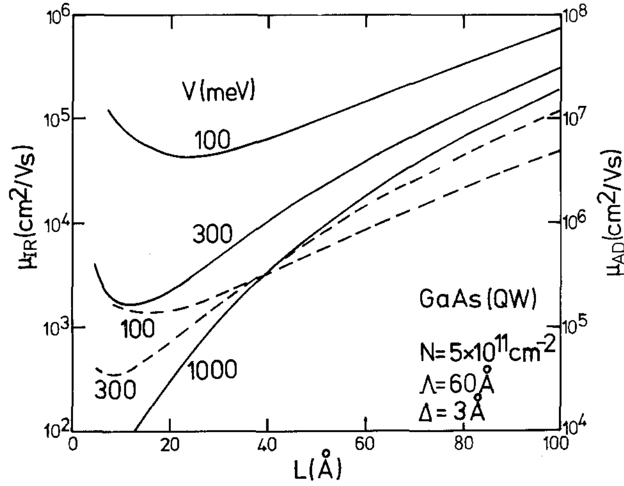


**Fig. 8.** Mobility $\mu$ versus QW width $L$ for interface-roughness scattering as solid lines (scale on the right hand side) and for alloy-disorder scattering as dashed lines (scale on the left hand side) according to (13a), (14), (18a), (19), (28) for various values of the confinement

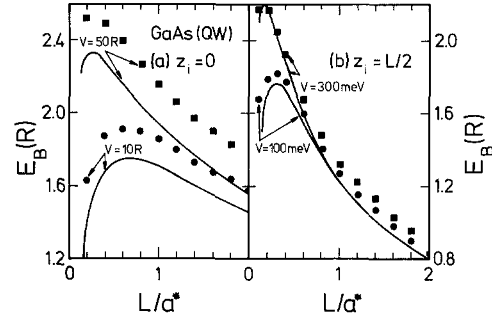


**Fig. 9.** Binding energy $E_B$ of unscreened hydrogenic impurities versus QW width $L$ according to (6), (7), (34) for impurities located in the center ($z_i=0$) and on the edge ($z_i=L/2$) of the QW. Squares and dots for $z_i=0$ are theoretical results of Greene and Bajaj [13] and Liu and Quinn [16], respectively. Squares and dots for $z_i=L/2$ are theoretical results of Mailhiot et al. [12]

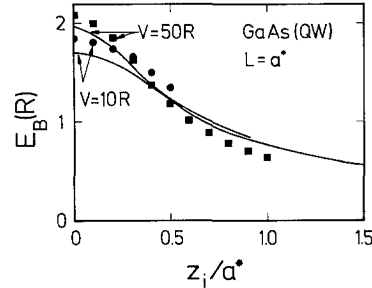


**Fig. 10.** Binding energy $E_B$ of unscreened hydrogenic impurities according to (6), (7), (34) versus impurity position $z_i$ as the solid line. The squares and dots are theoretical results of Liu and Quinn [16]

We mention that our results on the mobility are derived within Born's approximation. Multiple scattering effects which could lead to a metal-insulator transition [4] have been neglected.

### C. Binding energies for hydrogenic impurities

The calculation of the binding energy of hydrogenic impurities in QW's via variational wave functions has attracted much attention during the last years. Unscreened [12–14, 16, 17] and screened [15, 30] impurities have been considered. A different approach has been developed in [19]. The density of states calculations in the SPA provide the binding energy $E_B$ (measured from the bottom of the subband edge) for $N_i \to 0$ as the solution of the equation [19]

$$\frac{1}{\pi^2}\int_0^\infty dq\,q\,\frac{V_{ei,1}(q, V, L, z_i)}{\varepsilon(q, V, L)}\,\frac{1}{E_B+q^2/2m^*}=1. \tag{34}$$

For QW's with infinite barriers reasonable agreement with variational calculations on unscreened impurities [17] and screened impurities [15] has been obtained [20].

The binding energy versus QW width is shown in Fig. 9 for unscreened ($\varepsilon(q, V, L)=1$) impurities located in the center of the QW (Fig. 9a) and on the edge of the QW (Fig. 9b) for two different values of the confinement. With decreasing $L$ we find that $E_B$ first increases and then, after reaching a maximum, decreases. The decrease in $E_B$ with decreasing $L$ is a characteristic feature of finite barriers: For infinite barriers $E_B$ goes to $4R$ for $L\to 0$, the binding energy of the ideally two-dimensional system, whereas for finite barriers $E_B$ goes to $1R$ for $L\to 0$, the binding energy of the three-dimensional hydrogen atom [1, 17]. Our calculations are in full qualitative agreement and in good quantitative agreement (up to 10%) with the variational calculations of Greene and Bajaj [13] and Liu and Quinn [16] for $z_i=0$ (in the center) and of Mailhiot et al. [12] for $z_i=L/2$ (on the edge), which are also shown in Fig. 9. The maximum value of $E_B$ versus $L$ depends on $V$ and decreases with decreasing confinement, in agreement with the variational results.

In Fig. 10 the binding energies for unscreened impurities versus the location of the impurities are shown. Variational results of Liu and Quinn [16], which are also shown in Fig. 10, are in reasonable agreement with our calculation.

From theory [15, 30] and from experiment [31, 32] it is well known that the binding energy of hydrogenic impurities is strongly reduced by screening. The binding energy versus electron density for screened

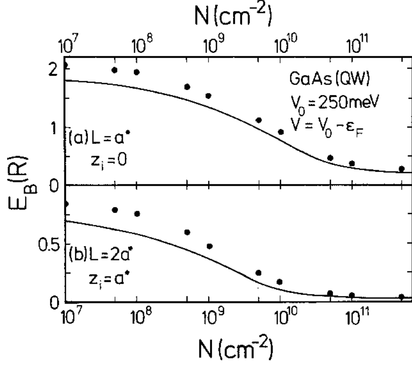


**Fig. 11a and b.** Binding energy $E_B$ of screened hydrogenic impurities according to (6), (7), (26), (34) versus electron density $N$ for impurities located (**a**) in the center and (**b**) on the edge of the QW. The dots are theoretical results of Guillemot [30]

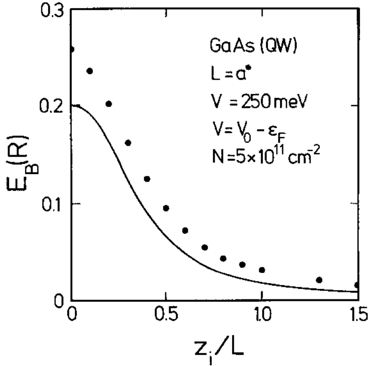


**Fig. 12.** Binding energy $E_B$ of screened hydrogenic impurities according to (6), (7), (26), (34) versus impurity position $z_i$ as the solid line. Dots are theoretical results of Guillemot [30]

impurities is shown in Fig. 11. We used Eq. (26) for $\varepsilon(q, V, L)$, which has the right property: $\varepsilon(q>0, V, L) = 1$ for $N \to 0$. The transition from screened impurities to unscreened impurities with $N \to 0$ is clearly seen in Fig. 11, where the binding energy increases with decreasing $N$. Variational results of Guillemot [30] for finite confinement are in reasonable agreement with our calculations on impurities located in the center (Fig. 11a) and on the edge (Fig. 11b) of the QW. We mention that we have accounted for the Pauli principle in the calculation shown in Fig. 11 as well as in Fig. 12; and $\varepsilon_F = 3.6$ meV$*(N/10^{11}$ cm$^{-2})$.

$E_B$ versus the position of the screened impurity for $N = 5*10^{11}$ cm$^{-2}$ is shown in Fig. 12. Our calculation is in good qualitative agreement with the variational calculation of Guillemot [30], which is also shown in Fig. 12. For impurities located in the barrier $E_B$ is strongly reduced in comparison to impurities located in the center of the QW.

We want to stress that the good agreement of the calculated binding energies according to (34) with the variational results, which we have demonstrated in Figs. 9–12, indicates that our approach can also be used for confinements other than square-well confinements for a reasonable estimate of the binding energy and the various dependences on impurity position, screening and confining parameters.

For unscreened impurities Eqs. (6, 34) can be rewritten as

$$\varepsilon_B^{1/2} = \frac{4}{\pi} \int_{-\infty}^{+\infty} dz |\Phi_1(V, L, z)|^2 \{\mathrm{ci}[\varepsilon_B^{1/2}|z-z_i|/a^*] \cdot \sin[\varepsilon_B^{1/2}|z-z_i|/a^*] - \mathrm{si}[\varepsilon_B^{1/2}|z-z_i|/a^*] \cdot \cos[\varepsilon_B^{1/2}|z-z_i|/a^*]\} \quad (35)$$

and $\varepsilon_B$ is the binding energy in effective Rydberg: $\varepsilon_B = E_B/R$. si$(x)$ and ci$(x)$ are the sine-integral and cosine-integral, respectively. Equation (35) should be useful in cases where an analytical expression for $F_{ei,1}(q, V, L, z_i)$ is not available and the wave function has been calculated numerically.

Resonant Raman scattering experiments on QW's have been interpreted as the observation of transitions from the ground impurity level of the first (ground) subband to the ground impurity level of the second and third subband [33]. These impurity states from higher subbands ("resonant impurity-states") overlap in energy with the continuum of the lowest subband and have been predicted in [34]. The good agreement of our calculated binding energy for the ground impurity level of the first subband with the variational calculations motivated us to study the binding energies of the higher subbands. In our calculation of the binding energies for impurities in higher subbands we neglect the interaction with the continuum of the lower subbands. It has been shown in [34, 35] that this is a very good approximation.

We used (34) and replaced $V_{ei,1}(q, V, L, z_i)$ by $V_{ei,n}(q, V, L, z_i)$. Unscreened impurities are assumed. $E_B$ is the binding energy measured form the $n$-th subband edge. Results for $E_B$ versus QW width for impurities located in the center of the well and for subbands $n = 1, 2, 3, 4$ are shown in Fig. 13. The binding energies decrease with increasing $n$. However, the binding energies for the third subband and $L > a^*$ are higher than for the second subband. This is due to the fact that the wave function (see (3b)), for $n = 2$ is zero for $z = 0$, and the electron-impurity interaction potential is weaker than in case of $n = 1$ and $n = 3$. A similar argument explains the higher binding energy of the fourth subband for $L > 1.7a^*$ in comparison to the second subband. With decreasing QW width the subband energies increase and subbands ($n \geq 2$) become

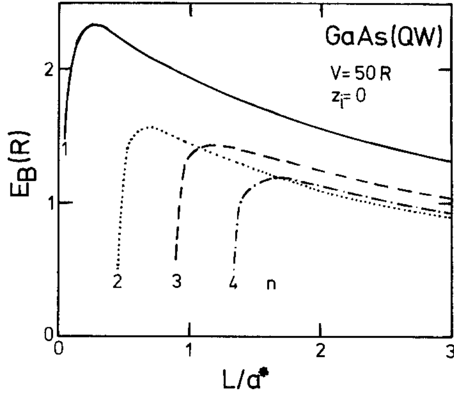


**Fig. 13.** Binding energy $E_B$ of unscreened hydrogenic impurities located in the center of the well versus QW width $L$ for subbands $n=1$, 2, 3, 4. We used (34) where we replaced $V_{ei,1}(q, V, L, z_i)$ by $V_{ei,n}(q, V, L, z_i)$ (see Eqs. (6), (7), (8))

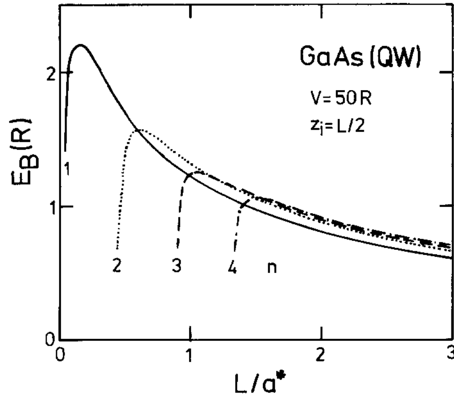


**Fig. 14.** Binding energy $E_B$ of unscreened hydrogenic impurities located on the edge of the well versus QW width for subbands $n=1$, 2, 3, 4. We used (34) where we replaced $V_{ei,1}(q, V, L, z_i)$ by $V_{ei,n}(q, V, L, z_i)$ (see Eqs. (6), (7), (8))

unconfined for $L \leqq L_n^* = a^* \pi (n-1)(m^* R/m_z V)^{1/2}$. Consequently the binding energy of hydrogenic impurities becomes zero for $L \leqq L_n^*$. Our results are in good agreement with the theoretical results of Ref. 34 for infinite confinement and of [35] for finite confinement.

In Fig. 14 the binding energy associated with subbands $n=1$, 2, 3, 4 versus QW width is shown for impurities located on the edge of the QW. For $L \gg L_n^*$ the binding energies for $n=2$, 3, 4 are larger than for $n=1$ due to the maximas of the wave function at $z>0$ for $n=2$, 3, 4 and the stronger electron-impurity interaction than for $n=1$. However, the differences between the binding energies are much smaller for impurities located on the edge of the QW than for impurities located in the center of the QW, compare Fig. 13 with 14.

## IV. Conclusion

We have given analytical expressions for the electron-impurity interaction potential, the electron-electron interaction potential, the interface-roughness scattering potential, and the alloy-disorder scattering potential for QW's with finite square-well confinement. With these expressions we discussed the influence of finite barriers on screening properties and on transport properties for impurity scattering, interface-roughness scattering, and alloy-disorder scattering. The comparison of our calculated binding energies of hydrogenic impurities (unscreened and screened) with the results of variational calculations indicates that our method could also be used to calculate the binding energy in geometries other than the square-well confinement.

The strongest effects of the finite confinement in comparison to the infinite confinement are found for the interface-roughness scattering, the alloy-disorder scattering (in the barrier), and the binding energy of shallow impurities in thin QW's. The penetration of the wave function into the barrier reduces the interface-roughness scattering and drastically enhances the alloy-disorder scattering. Interface-roughness scattering is found to be more important than alloy-disorder scattering. A non-monotonic behavior of the binding energy versus QW width is found, in agreement with the variational calculations [12–14, 16]. The binding energies of shallow impurities in higher subbands are also calculated.

I would like to thank G. Abstreiter, A. Ghazali, F. Koch, and J. Serre for valuable discussions. This work was supported by the Deutsche Forschungsgemeinschaft (Bonn).

## References

1. Ando, T., Fowler, A.B., Stern, F.: Rev. Mod. Phys. **54**, 437 (1982)
2. Linh, N.T.: Festkörperprobleme. Advances in solid state physics. Grosse, P. (ed.) Vol. 23, p. 227. Braunschweig: Vieweg 1983
3. Mori, S., Ando, T.: J. Phys. Soc. Jpn. **48**, 865 (1980)
4. Gold, A.: Solid State Commun. **60**, 531 (1986); Phys. Rev. B**35**, 723 (1987); Z. Phys. B – Condensed Matter **71**, 295 (1988)
5. Guillemot, C., Baudet, M., Gauneau, M., Regreny, A., Portal, J.C.: Phys. Rev. B**35**, 2799 (1987)
6. Cho, N.M., Ogale, S.B., Madhukar, A.: Phys. Rev. B**36**, 6472 (1987)
7. Stern, F., Howard, W.E.: Phys. Rev. **163**, 816 (1967)
8. Gottinger, R., Gold, A., Abstreiter, G., Weimann, G., Schlapp, W.: Europhys. Lett. **6**, 183 (1988)
9. Sakaki, H., Noda, T., Hirakawa, K., Tanaka, M., Matsusue, T.: Appl. Phys. Lett. **51**, 1934 (1987)
10. Ando, T.: J. Phys. Soc. Jpn. **51**, 3900 (1982)
11. Brum, J.A., Bastard, G.: Solid State Commun. **53**, 727 (1985)
12. Mailhoit, C., Chang, Y.-C., Mc Gill, T.C.: Surf. Sci. **113**, 161 (1982); Phys. Rev. B**26**, 4449 (1982)
13. Greene, R.L., Bajaj, K.K.: Solid State Commun. **45**, 825 (1983)
14. Tanaka, K., Nakaoka, M., Yamabe, T.: Phys. Rev. B**28**, 7068 (1983)

15. Brum, J.A., Bastard, G., Guillemot, C.: Phys. Rev. B **30**, 905 (1984)
16. Liu, W., Quinn, J.J.: Phys. Rev. B **31**, 2348 (1985)
17. Bastard, G.: Phys. Rev. B **24**, 4714 (1981)
18. Delalande, C.: Physica **146** B, 112 (1987);
Shanabrook, B.V.: Physica **146** B, 121 (1987);
Mc Combe, B.D., Jarosik, N.J., Mercy, J.-M.: In: Two-dimensional systems: physics and new devices. Bauer, G., Kuchar, F., Heinrich, H. (ed.), p. 156. Berlin, Heidelberg, New York: Springer 1986
19. Gold, A., Serre, J., Ghazali, A.: Phys. Rev. B **37**, 4589 (1988);
Ghazali, A., Gold, A., Serre, J.: Surf. Sci. **196**, 346 (1988)
20. Serre, J., Ghazali, A., Gold, A.: Phys. Rev. B (submitted for publication);
Gold, A., Serre, J., Ghazali, A.: Presented at the "19th International Conference on the Physics of Semiconductors", Warshaw, August (1988), (in press)
21. Harrang, J.P., Higgins, R.J., Goodall, R.K.: Jay, P.R., Laviron, M., Delescluse, P.: Phys. Rev. B **32**, 8126 (1985)
22. Das Sarma, S., Stern, F.: Phys. Rev. B **32**, 8442 (1985)
23. Gold, A.: Phys. Rev. B **38**, 10798 (1988)
24. Prange, R.E., Nee, T.W.: Phys. Rev. **168**, 779 (1968)
25. Price, P.J., Stern, F.: Surf. Sci. **132**, 577 (1983)
26. Stern, F.: Phys. Rev. Lett. **18**, 546 (1967)
27. Jonson, M.: J. Phys. C **9**, 3055 (1976)
28. Gold, A., Dolgopolov, V.T.: Phys. Rev. B **33**, 1076 (1986)
29. Cho, N.M., Ogale, S.B., Madhukar, M.: Appl. Phys. Lett. **51**, 1016 (1987)
30. Guillemot, C.: Phys. Rev. B **31**, 1428 (1985)
31. Zawadzki, W., Kubisa, M., Raymond, A., Robert, J.L., Andre, J.P.: Phys. Rev. B **36**, 9297 (1987)
32. Gammon, D., Glaser, E., Shanabrook, B.V., Musser, D.: Surf. Sci. **196**, 359 (1988)
33. Perry, T.A., Merlin, R., Shanabrook, B.V., Comas, J.: Phys. Rev. Lett. **54**, 2623 (1985)
34. Priester, C., Allan, G., Lannoo, M.: Phys. Rev. B **29**, 3408 (1984)
35. Jayakumar, K., Balasubramanian, S., Tomak, M.: Phys. Rev. B **34**, 8794 (1986)

A. Gold
Groupe de Physique des
Solides de l'Ecole Normale Supérieure
Université Paris 7
Tour 23, 2 place Jussieu
F-75251 Paris 5
France